

Fabrication of composite nanofiltration membranes by dopamine-assisted poly(ethylene imine) deposition and cross-linking^{*}

Pei-bin ZHANG, Cui-jing LIU, Jian SUN, Bao-ku ZHU, Li-ping ZHU^{†‡}

(MOE Key Laboratory of Macromolecule Synthesis and Functionalization, Department of Polymer Science and Engineering,
 Zhejiang University, Hangzhou 310027, China)

[†]E-mail: lpzhu@zju.edu.cn

Received Apr. 23, 2016; Revision accepted Nov. 9, 2016; Crosschecked Jan. 6, 2017

Abstract: Positively charged composite nanofiltration (NF) membranes with good stability were prepared by dopamine (DA) assisted poly(ethylene imine) (PEI) deposition on a polysulfone ultrafiltration (UF) substrate followed by a cross-linking step. Attenuated total reflectance Fourier transform infrared spectroscopy, X-ray photoelectron spectroscopy, scanning electronic microscopy, and atom force microscopy were employed to characterize the surface chemistry and morphology of the obtained composite membranes. The DA and PEI co-deposition conditions were optimized based on knowledge of the co-deposition mechanism. The effects of the cross-linker concentration, cross-linking time, and reaction temperature on the permeation and separation properties of the prepared composite membranes were investigated in detail. Under optimized conditions, the MgCl_2 rejection and permeation flux of the composite membrane reached 80.4% and $19.6 \text{ L}/(\text{m}^2 \cdot \text{h})$, respectively (the feed was 0.01 mol/L of MgCl_2 solution under a test pressure of 0.4 MPa). The rejection of various salts followed the order $\text{MgCl}_2 > \text{CaCl}_2 > \text{MgSO}_4 > \text{NaCl} > \text{Na}_2\text{SO}_4$, suggesting the membranes were positively charged. The composite membranes showed good durability under alkaline aqueous conditions. This study provided new insights into the fabrication of mussel-inspired thin-film composite nanofiltration membranes.

Key words: Dopamine (DA); Poly(ethylene imine) (PEI); Co-deposition; Nanofiltration (NF) membranes; Cross-linking
<http://dx.doi.org/10.1631/jzus.A1600308>

CLC number: TQ028.8

1 Introduction


Nanofiltration (NF) is a pressure-driven membrane process which is gaining increasing attention because of its higher permeation flux and lower energy consumption compared to reverse osmosis and its higher retention of multivalent ion salts compared to ultrafiltration (UF). NF has been widely used in water softening, waste water treatment, and the sep-

aration of small molecules like sugars, amino acids, and dyes (Bouchoux *et al.*, 2005; Ouyang *et al.*, 2008; Riera-Torres *et al.*, 2010). Generally, a surface charged NF membrane is more likely than a neutral membrane to reject the same charged multivalent ions, due to not only the steric hindrance effect (Szymczyk and Fievet, 2005), but also the electrostatic repulsive effect (Schaep and Vandecasteele, 2001).

At present, the active separation layer of most thin-film composite NF membranes is made of polyamide (PA) generated by an interfacial polymerization process. The PA layer is often negatively charged and appropriate for the separation of multivalent anions. However, in some applications, such as water softening, heavy metal removal, and the purification

^{*} Corresponding author

[†] Project supported by the National Natural Science Foundation of China (Nos. 51273176 and 51573159) and the Fundamental Research Funds for the Central Universities (No. 2016QNA4032), China

 ORCID: Li-ping ZHU, <http://orcid.org/0000-0002-1553-4190>

© Zhejiang University and Springer-Verlag Berlin Heidelberg 2017

of positively charged dyes, positively charged NF membranes are more favorable. In recent years, various methods have been developed to fabricate positively charged NF membranes including photo-initiated grafting (Akbari *et al.*, 2006; Li *et al.*, 2011b), layer-by-layer (LbL) deposition (Miller and Bruening, 2004; Chan *et al.*, 2012; Saeki *et al.*, 2013), and chemical cross-linking (Zhou *et al.*, 2007; Vanherck *et al.*, 2008; Ji *et al.*, 2012; Feng *et al.*, 2014). However, these techniques have shortcomings. For instance, the ultraviolet (UV)-induced grafting method is limited by possible damage to the substrates due to the cleavage of chemical bonds. LbL deposition is a multistep process that is sophisticated and difficult to scale up. In contrast, chemical cross-linking is a simple and feasible strategy to fabricate a dense selective layer of a composite NF membrane. But the attachment of the cross-linked surface layer to the porous support membrane needs further enhancement to realize stable and durable separation.

In recent years, mussel-inspired chemistry has attracted much attention as a universal strategy for material surface modification and chemical tailoring. It was reported that dopamine (DA), a typical mussel-inspired catecholic molecule, can undergo a complicated oxidation, cross-linking and self-assembly process under weak alkaline conditions (Lee *et al.*, 2007) and generate a robust polydopamine (PDA) coating on various materials without causing damage. Numerous studies have been published on the surface modification of solid materials using DA for different purposes like improving hydrophilicity (Jiang *et al.*, 2011) and anti-fouling ability (Kasemset *et al.*, 2013), enhancing surface coating stability (Chen *et al.*, 2009; Cheng *et al.*, 2013), and further functionalization (Jiang *et al.*, 2010; Zhao *et al.*, 2014). Recently we have fabricated a novel NF membrane based on multiple deposition procedures of PDA onto a polysulfone (PSf) UF membrane (Li *et al.*, 2011a). To improve the performance of the PDA NF membrane, Li *et al.* (2014) prepared an NF membrane by a multistep sequential process consisting of the deposition of DA, grafting of PEI and chemical cross-linking. Kang *et al.* (2012) reported multipurpose surface functionalization through one step co-deposition of DA and other functional molecules, introducing a more convenient approach to surface modification of functional materials. Previous work on PDA NF membranes has

shown that the PDA separation layer demonstrates good stability in a mild environment, as neat PDA or a PDA-contained layer can attach to a porous support membrane. However, the poor tolerance of PDA to alkali limits the application of PDA NF membranes.

The objective of this study was to prepare highly alkali tolerant PDA NF membranes by DA-assisted PEI deposition onto PSf UF membranes and further cross-linking using epichlorohydrin (ECH) (Fig. 1). The effects of the co-deposition and cross-linking conditions on NF performance were investigated in detail. We hoped to establish a feasible method to improve the durability of DA-modified membranes during the NF process and chemical washing.

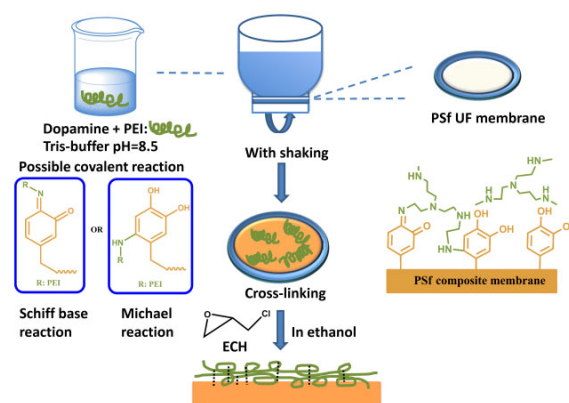


Fig. 1 Experimental process and possible reaction mechanism of PEI and DA co-deposition and further cross-linking using ECH

2 Materials and methods

2.1 Materials and reagents

Polysulfone (PSf) flat-sheet UF (molecular weight cut-off at 70 kDa) membranes were provided by Vontron Technology Co., Ltd. (China) and preserved in 1% (weight concentration, the same meaning unless otherwise stated) sodium hydrogen sulfite solution. 3,4-dihydroxyphenethylamine (dopamine) was purchased from Sigma-Aldrich (China) and used as received. Branched poly(ethylene imine) (PEI; 99%, $M_w=10000$) was purchased from Alfa Aesar (China). Epichlorohydrin (ECH), magnesium chloride ($MgCl_2$), magnesium sulfate ($MgSO_4$), sodium sulfate (Na_2SO_4), sodium chloride ($NaCl$), sodium hydroxide ($NaOH$), hydrochloric acid (HCl), tris(hydroxymethyl) aminomethane (Tris) and a series

of polyethylene glycols (PEGs; $M_w=200\text{--}3000$ Da) were analytical grade and obtained from the Sinopharm Chemical Reagent Co. (Shanghai, China). VB_{12} was obtained from the Aladdin Industry Co. (Shanghai, China). Ultrapure water was produced by a Millipore direct-Q system (USA).

2.2 Membrane preparation

DA-assisted PEI deposition onto the PSf membrane surface was carried out using a fixed bottle cap to make sure that only the upside of the membrane was incubated in solution. The PSf membrane was washed with ultrapure water three times before use to remove residual sodium hydrogen sulfite from the membrane. An aqueous solution for co-deposition was prepared by dissolving DA and PEI in tris-buffer solution (pH=8.5, 50 mmol/L). After immersion for 24 h, the composite membrane, named PSf-PEI/PDA, was taken out and rinsed with ultrapure water to remove loosely combined molecules. Then ECH, as a cross-linker, at different concentrations in ethanol was applied to further modify the composite membrane. The interfacial cross-linking reaction was carried out at different temperatures and for different time periods. Afterwards, the composite membranes, denoted as PSf-PEI/PDA/ECH, were washed with ultrapure water by vibration to remove the unreacted ethanol and ECH. Finally, the membranes were stored in ultrapure water for further study.

2.3 Membrane characterization

The surface chemical composition of pristine PSf and the composite membranes was tested by X-ray photoelectron spectroscopy (XPS; PHI 5000C ESCA system, USA) with Mg K α excitation radiation ($h\nu=1253.6$ eV). Attenuated total reflectance Fourier transform infrared spectra (ATR-FTIR; Nicolet 6700, USA) were employed to analyze and compare the functional groups of the membrane surface before and after deposition and cross-linking. The surface hydrophilicities of the membranes were characterized by water contact angle measurement (CA, OCA20, Dataphysics, Germany). A volume of 1 μL of ultrapure water was dropped onto the dry membrane surface.

The surface morphologies were observed by field emitting scanning electronic microscopy (FESEM; Hitachi S-4800, Japan) and atomic force microscopy (AFM; SPI3800N, Seiko Instrumental,

Japan). AFM images were recorded in the tapping mode with silicone tip cantilevers having a force constant of 40 mN/cm and scanned in a $5\text{ }\mu\text{m}\times 5\text{ }\mu\text{m}$ area. Root mean square (RMS) roughness values were calculated to express the surface roughness.

The surface charge properties were determined by a streaming potential method. The zeta potential was measured by an electrokinetic analyzer (SurPASS Anton Paar, GmbH, Austria) and the value of the zeta potential ζ was calculated using the Helmholtz-Smoluchowski equation:

$$\zeta = \frac{\Delta E}{\Delta P} \frac{\eta \kappa}{\varepsilon}, \quad (1)$$

where ΔE is the streaming potential difference, ΔP is the pressure difference, ε is the dielectric constant, and η and κ are the viscosity and the conductivity, respectively, of the solution.

2.4 Evaluation of NF performance and stability

Separation performance tests were carried out under 0.4 MPa pressure using a dead-end solvent resistant stirred cell (Millipore Co., USA) with an effective area of 15 cm^2 . N_2 was introduced to maintain a constant pressure. For the filtration tests, all the membrane samples were first pre-pressured under a designated pressure with ultrapure water as feed for 0.5 h. For each separation test, the water flux recorded was the averaged value of three parallel experiments. The permeation flux (F) was calculated by

$$F = \frac{V}{At}, \quad (2)$$

where V is the total value volume of permeate during the operating time t , and A is the membrane area.

After water permeation measurements, various inorganic salts (MgCl_2 , CaCl_2 , NaCl , Na_2SO_4 , and MgSO_4) and neutral solutes (VB_{12} and PEGs 200–3000 Da) were used as feed solutions to evaluate the separation performance. The concentration of feed solution was 0.01 mol/L of salts, 0.1 g/L of VB_{12} and 0.5 g/L of PEGs. The salt concentration was measured by an electrical conductivity meter (DDS-11A, Shanghai Leici Instrument, China), VB_{12} by a UV/vis spectrophotometer (UV5500-PC, Shanghai Jingke Instrument, China) and PEGs by a

total organic carbon (TOC) analyzer (Analytik Jena Multi N/C 3000, Jena, Germany). The observed rejection ratio (R_{obs}) of the solute was calculated by

$$R_{\text{obs}} = \left(1 - \frac{C_p}{C_r}\right) \times 100\%, \quad (3)$$

where C_p and C_r represent the concentrations of the permeate and the feed solution, respectively. The real solute rejection (R_{real}) for membranes can be calculated using a mass transfer correlation procedure (Bowen *et al.*, 1997).

$$\ln\left(\frac{1 - R_{\text{obs}}}{R_{\text{obs}}}\right) = \ln\left(\frac{1 - R_{\text{real}}}{R_{\text{real}}}\right) + \frac{J_v}{k}, \quad (4)$$

where J_v is the volume of flux (m/s), and k is the mass transfer coefficient. The k value of the solvent resistant stirred cell was 2×10^{-5} based on the mass transfer correlation prediction (Zeman and Zydney, 1996).

The average pore size, d_p , for the composite NF membranes can be approximated using the pore-flow model by conducting VB₁₂ filtration tests at different permeate fluxes (Bowen *et al.*, 1997; Nghiem *et al.*, 2004). The d_p was determined by fitting the real rejection data to the model (Eq. (5)) using an optimization procedure (Solver, Microsoft Excel).

$$R_{\text{real}} = 1 - \frac{C_p}{C_m} = 1 - \frac{\Phi K_c}{1 - \exp(-Pe_m)(1 - \Phi K_d)}, \quad (5)$$

where C_m and C_p are the external solute concentrations on the feed side and permeate side of the membrane, respectively. K_d and K_c are the diffusion and convection mass transfer coefficient, respectively. $\Phi = (1 - \lambda)^2$ is the equilibrium partition coefficient, λ is the ratio of solute diameter to pore diameter, and $\lambda = d_s/d_p$. d_s is the diameter of solute. Pe_m is the Peclet number.

The pore-flow model assumes porous NF membranes consist of bundles of cylindrical capillary tubes with the same radius. The ratio of membrane thickness to porosity, $\Delta x/A_k$, can also be approximated based on water permeance according to the Hagen-Poiseuille equation:

$$J_v = \frac{d_p^2 \Delta P}{32\eta(\Delta x / A_k)}, \quad (6)$$

where η is the water viscosity (0.00089 Pa·s), Δx the effective membrane thickness (μm), and A_k the porosity of the membrane.

The pore size distribution of the composite membranes was calculated by applying a solute transport method based on the apparent rejections of PEGs with different molecular weights, as described by Singh *et al.* (1998) and van der Bruggen *et al.* (2000). The mean effective pore diameter (μ_p) and the geometric standard deviation (σ_p) can be determined. Therefore, the pore size distribution can be expressed by the probability density function in the following equation:

$$\frac{dR(r_p)}{dr_p} = \frac{1}{r_p \ln \sigma_p \sqrt{2\pi}} \exp\left[-\frac{(\ln r_p - \ln \mu_p)^2}{2(\ln \sigma_p)^2}\right], \quad (7)$$

where r_p is the membrane pore size.

Long-term flux and rejection tests were conducted for several days to investigate the stability of the composite membrane.

3 Results and discussion

3.1 DA-assisted PEI deposition on PSf substrate

In a weak alkaline aqueous solution, DA can undergo a self-polymerization process to form a thin PDA film on various substrate surfaces (Lee *et al.*, 2007). This phenomenon gave rise to a new method for surface modification of solid materials. The catechol group in DA can be oxidized to become a quinone form, which can potentially react with an amino or thiol group via the Michael addition or Schiff base reaction (Xu *et al.*, 2010). Based on this reaction, we prepared composite NF membranes via DA-assisted PEI deposition followed by a cross-linking step using ECH.

To prepare the composite NF membranes, the conditions of co-deposition of DA and PEI were first investigated. The concentration of DA was chosen as 1.0 g/L, which was a conventional amount used for modification. Over a period of 24 h of co-deposition,

the effects of various PEI concentrations and temperatures on NF performance were investigated. Without PEI deposition, the composite membrane showed a low rejection of MgCl_2 (Table 1). The PDA coating layer may not have been dense enough to cover all the pores of the PSf membrane, which depends mainly on the pore size distribution of the substrate. We concluded that co-deposition with 1.0 g/L of PEI was appropriate to obtain a membrane with relatively high MgCl_2 retention, as lower or higher concentrations of PEI had little effect on the membrane's performance. The manner of co-deposition in solution could help us better understand the mechanism of the DA-assisted deposition process on the membrane surface. Precipitation of DA solution in the absence of PEI can be seen only after centrifugation. When PEI at a concentration lower than 1.0 g/L was co-deposited with DA, the aggregates that formed had a relatively large size and could be seen at the bottom of the solution after standing. This may have been because DA assembly occurred with branched PEI via covalent or non-covalent interactions to form large cross-linked aggregates in solution. As the concentration increased to 3.0 g/L and 5.0 g/L, the precipitations disappeared and the color of the solution lightened compared with PDA solution. The color on the obverse side of the membranes also turned lighter with increasing PEI concentration (Fig. 2). These phenomena suggested that access to PEI can greatly influence the DA self-polymerization and self-assembly process, and directly affect the manner of deposition of both components onto the PSf substrate. This supports the results of a recent study which showed that amine-containing buffer solution shows covalent incorporation with DA oligomers (Della Vecchia *et al.*, 2013). Increasing temperature resulted in a better NF performance of the composite membrane. This can be explained by the higher temperatures causing more aggregates to be deposited on the membranes (Jiang *et al.*, 2011) and increasing the reactivity of the Michael addition and Schiff base reaction.

In consideration of the better NF performance of the composite membranes, a composite membrane prepared by co-deposition of DA and PEI, each at a concentration of 1.0 g/L, at under 60 °C, was chosen for further cross-linking. ECH was applied here, as it can react with both DA and PEI (Li *et al.*, 2014).

Table 1 Separation performance of composite membranes prepared in various co-deposition conditions (the concentration of DA was 1.0 g/L)

C_{PEI} (g/L)	Temperature (°C)	Flux (L/(m ² ·h))	Rejection (%)
Pristine PSf	25	720.6±37.8	0
0	25	92.8±2.8	4.4±1.3
0.1	25	202.0±4.7	3.8±0.7
0.2	25	211.6±3.3	3.5±0.9
0.5	25	214.0±1.2	8.9±0.2
1.0	25	54.4±2.8	18.9±0.6
3.0	25	292.8±4.8	11.7±0.6
5.0	25	361.2±3.6	6.0±1.0
1.0	40	57.1±0.9	20.1±0.6
1.0	60	59.7±5.2	32.0±0.8

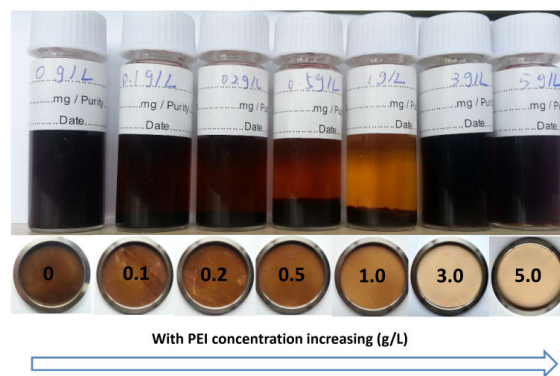


Fig. 2 A digital photograph of co-deposition solutions and obverse sides of PSf-PEI/PDA membranes with increasing concentrations of PEI

3.2 Membrane surface chemistry, morphology, and physiochemical characteristics

To confirm that PEI was deposited on the PSf membrane during the co-deposition process, the changes in surface chemical functional groups were analyzed by ATR-FTIR spectra (Fig. 3a). Compared with the pristine PSf membrane and the PSf-PDA composite membrane, a new absorption signal at 1656 cm^{-1} was observed in PSf-PEI/PDA composite membranes. This peak corresponds to the formation of C=N bonds between PEI and DA (Yang *et al.*, 2014). The IR absorption of N-H bending vibrations and C=C resonance vibrations in aromatic rings overlapped at 1600 cm^{-1} in both DA and DA-assisted deposition membranes. In consideration of the different atomic ratios of PEI and PDA, XPS analysis was more effective in determining the surface chemical composition of the different membranes.

The appearance of an N 1s peak in the pristine PSf membrane (Fig. 3b) may have been due to the addition of a pore-forming agent in the fabrication process. After the deposition of DA, an obvious increase in the percentage of nitrogen was observed (Table 2) and the N/C ratio (0.120) was similar to the theoretical value of the N/C ratio of DA (0.125). When PEI co-deposited with DA, the N/C ratio increased from 0.120 in the PSf-PDA composite membrane to 0.169 in the PSf-PEI/PDA composite membrane, indicating that PEI was successfully deposited on the PSf membrane with the aid of DA. Both the N/C and N/O ratios increased after cross-linking compared to the corresponding values before cross-linking, which may be explained by the adjustment of chain conformation of PEI and PDA during the cross-linking reaction.

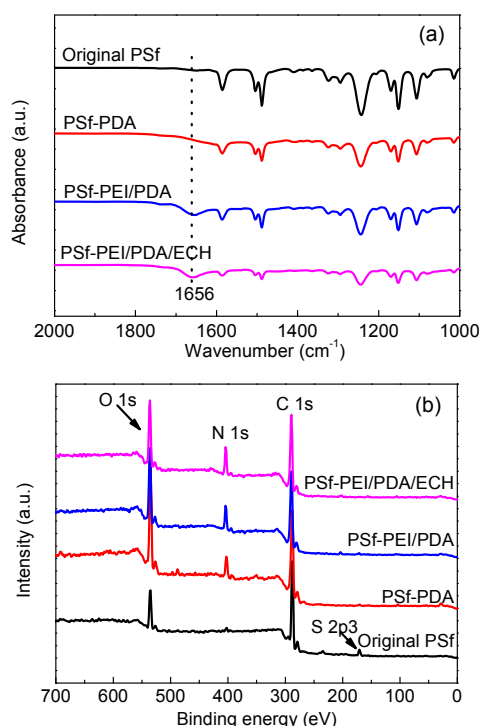


Fig. 3 (a) ATR-FTIR spectra of the studied membranes; (b) Typical XPS wide scans for the studied membranes

The surface morphologies of the PSf membrane, PSf-PEI/PDA, and PSf-PEI/PDA/ECH composite membranes were examined by FESEM. The pristine PSf membrane had a smooth surface with pores. After co-deposition of PEI and DA, the surface of the membrane was covered with many more aggregates, supporting the results of Chien *et al.* (2013) with DA-assisted surface modification. The aggregates formed here presumably resulted from PEI participating in the self-oxidation and self-assembly of DA. PEI with a branched structure may have formed a cross-linking network with DA so that the deposition aggregates were larger than general PDA particles. Moreover, the cross-linker ECH may react with amino groups from PEI and PDA, leading to the coalescence of aggregates to form larger units. In addition, the high temperature (60 °C) for cross-linking may provide the conditions to adjust the conformation of the molecular chain, which is consistent with the XPS analysis results. The cross-linked composite membrane was dense and the pores were totally covered, indicating that it can be used in NF applications. The cross section SEM images in Fig. 4 show that the skin layer consisted of a dense layer and aggregated particles. The PSf-PDA composite membrane had a relatively thin layer of about 45 nm, consistent with the thickness of general PDA coatings (Jiang *et al.*, 2011). When introducing PEI into co-deposition followed by cross-linking, the covalent or non-covalent reaction between the individual components resulted in complex aggregates forming at the interfaces. The thicknesses of PSf-PEI/PDA and PSf-PEI/PDA/ECH composite membranes were 115 nm and 120 nm, respectively. AFM analysis was also carried out to investigate the morphology of the membrane surface at the nanoscopic scale. The AFM images with root mean square (RMS) roughness data are shown in Fig. 4. As observed in the SEM images, the roughness value became larger after co-deposition and the cross-linking reaction.

Table 2 Surface chemical composition from XPS analysis of PSf, PSf-PDA composite, PSf-PEI/PDA composite, and PSf-PEI/PDA/ECH composite membranes

Sample	Atomic percentage (% , mole concentration)					N/C	N/O
	C	O	N	S	Cl		
PSf	80.2	15.3	1.8	2.7	–	–	–
PSf-PDA	65.9	25.9	7.9	0.3	–	0.120	0.305
PSf-PEI/PDA	65.8	22.4	11.2	0.6	–	0.169	0.497
PSf-PEI/PDA/ECH	67.6	19.7	11.9	0.2	0.6	0.176	0.604

The surface hydrophilicity and wetting properties were characterized via water contact angle measurement. The curves of the contact angle decaying with time for the composite membranes are shown in Fig. 5. The contact angle of the pristine PSf membrane was about 95° and decreased by about 8° by 90 s, indicating poor hydrophilicity and wetting ability. After co-deposition of PEI/PDA, the contact angle decreased from 66° to 25° in 90 s, indicating that surface hydrophilicity had improved considerably. For the ECH cross-linked membrane, the initial contact angle value was 59° and the curves attenuated sharply, indicating a remarkable improvement in

surface hydrophilicity. This may have been the result of the hydrophilic groups $-\text{NH}_2$ from PEI and $-\text{OH}$ from ECH being successfully introduced to the membrane surface through the co-deposition and cross-linking steps, respectively. On the other hand, the surface roughness obviously increased and this enhanced roughness effect would benefit the solid/liquid/gas system in a contact angle test (Tian *et al.*, 2014).

The electrical properties of the membrane surface are represented by the zeta potential (Fig. 6). The isoelectric points of the original PSf and PSf-PDA composite membrane were at pH values of 4.6 and 5.1,

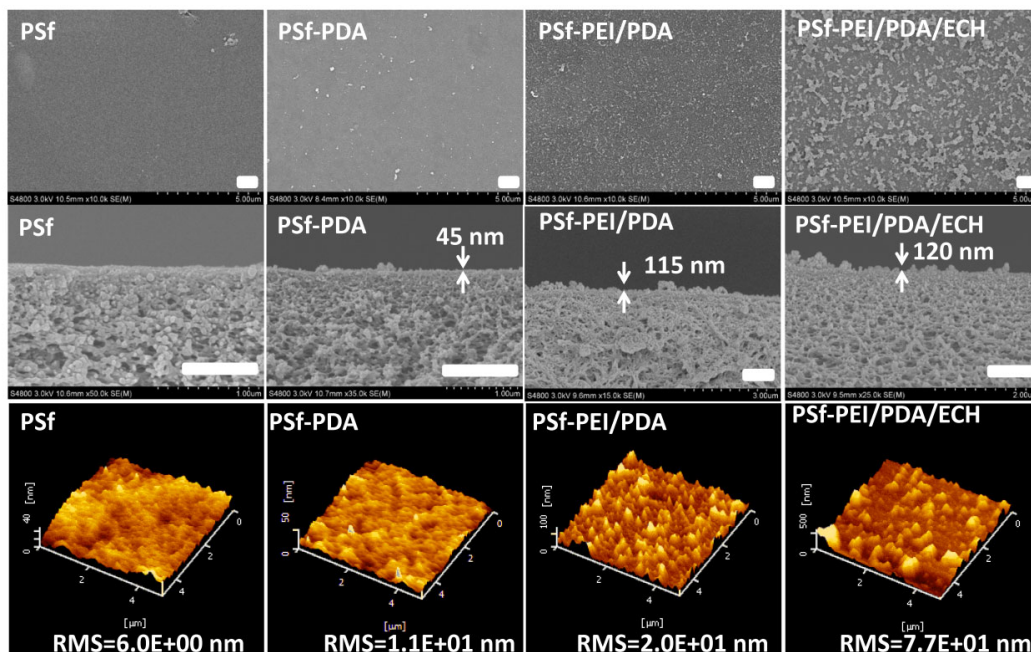


Fig. 4 FESEM images of the surfaces of the studied membranes and cross-section morphologies and AFM images of the surfaces of the composite membranes (all scale bars are 1 μm)

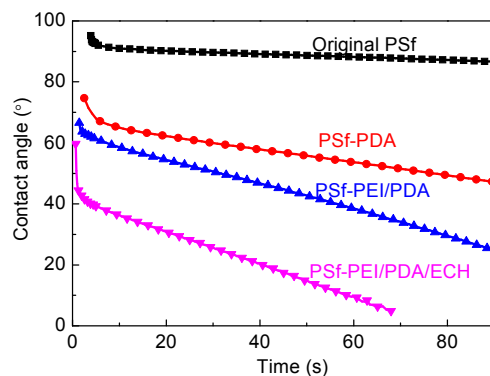


Fig. 5 Time dependence of the water contact angle of the studied membranes

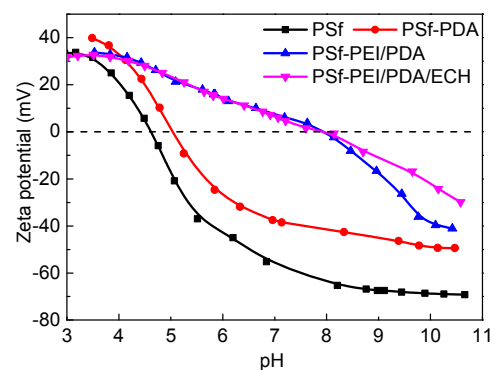


Fig. 6 Zeta potential of the studied membranes at various pH values

respectively. The introduction of PEI obviously raised the isoelectric points. Cross-linking by ECH did not have much effect on the surface electrical properties. The results from zeta potential suggest that the composite membranes were positively charged during the NF operation.

3.3 NF performances

During the cross-linking reaction, ECH was chosen to be the crosslinker as it can react with both DA and PEI via a nucleophilic substitution reaction. To illustrate the role of PEI in NF performance, the control membrane prepared only by DA deposition was firstly cross-linked by ECH. When the concentration of ECH was 10%, the PDA coating membrane showed a large flux decrease from 92.8 L/(m²·h) before cross-linking to 25.7 L/(m²·h) (at 0.4 MPa) after cross-linking. However, the rejection of MgCl₂ increased only from 4.4% to 8.7% compared to large decrease in flux, which may have been because the cross-linking between short PDA chains cannot effectively reduce the pore size of the membranes.

After co-deposition with PEI, a relatively long chain branched molecular structure, cross-linked by ECH, endows the composite membranes with a dense selective layer making them suitable for use as NF membranes. The influence of the ECH concentration on membrane performance was investigated with various concentrations of ECH from 1% to 15%. The cross-linking reaction was conducted at 60 °C for 24 h. The rejection of MgCl₂ by the composite membrane increased with the decreasing permeate flux (Fig. 7a). This could be attributed to the increased degree of cross-linking making the surface more dense. Interestingly, the PSf-PEI/PDA composite membrane showed a small increase in rejection of MgCl₂ after immersion in ethanol solution at 60 °C without ECH, suggesting that PEI and PDA had reactivity for further reactions in their own right. The rejection of MgCl₂ tended to level-off when the concentration of ECH exceeded 10%.

The effects of the cross-linking temperature and time on NF performance were also examined. We concluded that both temperature and time play

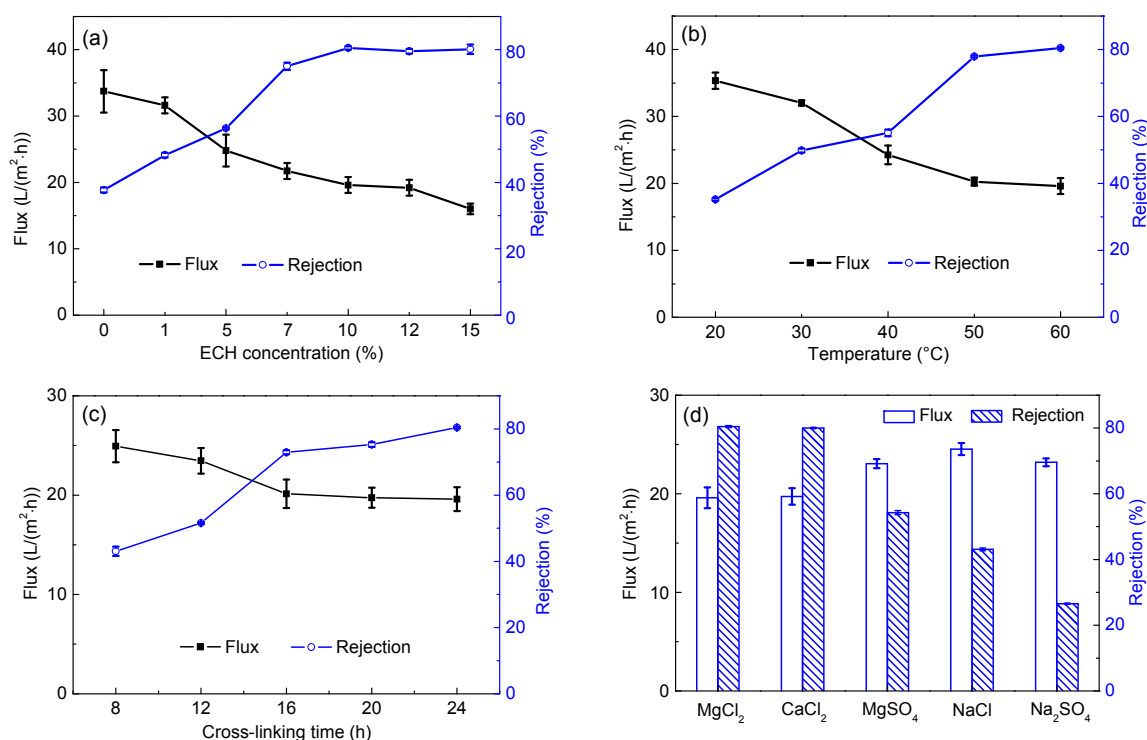


Fig. 7 (a) Effect of ECH concentration on NF performance of the composite membrane (the temperature and time were fixed at 60 °C and 24 h, respectively); (b) Effect of cross-linking temperature on NF performance (the ECH concentration and the reaction time were fixed at 10% and 24 h, respectively); (c) Effect of cross-linking time on NF performance (the ECH concentration and the reaction temperature were fixed at 10% and 60 °C, respectively); (d) Effect of the separation of different salts on NF performance. All salt solutions had a concentration of 0.01 mol/L under a pressure of 0.4 MPa

important roles in the cross-linking process. When an ECH concentration of 10% was selected, the rejection of MgCl_2 increased with increasing temperature and time (Figs. 7b and 7c). At a concentration of 10% at 60 °C for 24 h, the composite membrane showed 80.4% rejection of MgCl_2 , and permeate flux reached 19.6 $\text{L}/(\text{m}^2\cdot\text{h})$. Using the composite membrane, tests of rejection of different salts were conducted at a concentration of 0.01 mol/L. The order of rejection of different salts was $\text{MgCl}_2 \approx \text{CaCl}_2 > \text{MgSO}_4 > \text{NaCl} > \text{Na}_2\text{SO}_4$ (Fig. 7d). The order of $R(\text{MgCl}_2) > R(\text{NaCl})$ and $R(\text{MgSO}_4) > R(\text{Na}_2\text{SO}_4)$ can be explained by the Donnan exclusion theory that indicates a stronger electrostatic repulsive interaction between the divalent cations and the positively charged membrane surface (Schaep *et al.*, 1998). The rejection performance of NF membranes is also determined by steric hindrance, and both effects dictate a greater retention of MgSO_4 than NaCl .

To understand better the sieving mechanism of the composite membranes, tests of the real rejection rates of VB_{12} at different volume fluxes were conducted to evaluate the pore size, d_p , and the ratio of effective membrane thickness to porosity ($\Delta x/A_k$). Fig. 8a shows the real rejection rates of VB_{12} with various volume fluxes, and Table 3 shows d_p and $\Delta x/A_k$ calculated for typical membranes. It is obvious that the average pore size, d_p , decreased after ECH cross-linking from 2.53 nm to 1.68 nm. The values of $\Delta x/A_k$ increased after the cross-linking reaction. This may be attributed to the composite membranes becoming denser (smaller A_k).

In addition, another method using solute transport with PEG rejection was applied to evaluate pore size and pore size distribution. The mean effective pore diameter (μ_p), geometric standard deviation (σ_p), and pore size cutoff were also compared (Table 3). The pore size distribution and cumulative pore size distribution curves based on the values of μ_p and σ_p are presented in Figs. 8b and 8c. The value of μ_p can be considered to be the value of the geometric

mean diameter of the PEGs (μ_s) at 50% rejection, which was lower than d_p evaluated from VB_{12} rejection. The pore size cutoff from the PEG rejection data

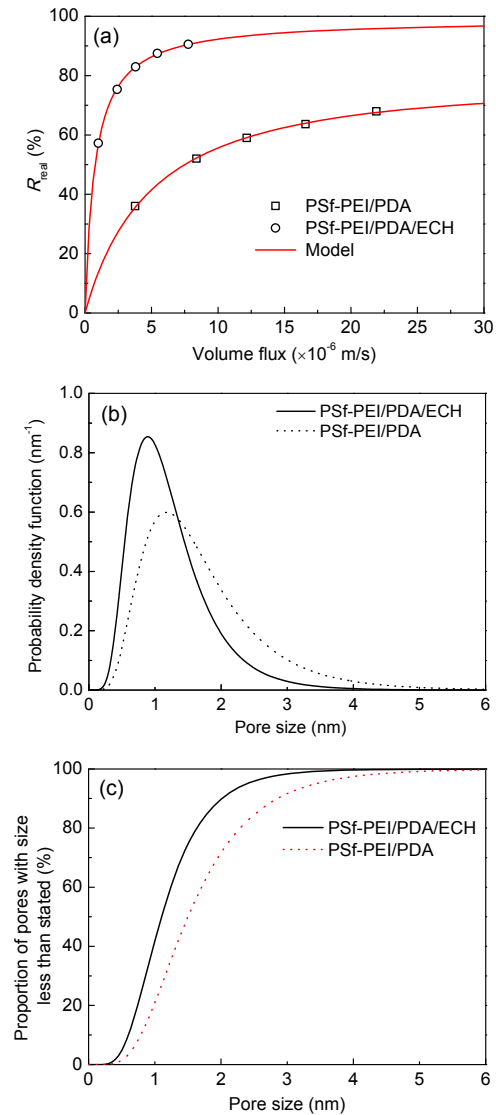


Fig. 8 (a) Real rejection rates for VB_{12} solution as a function of permeate flux for PSf-PEI/PDA and PSf-PEI/PDA/ECH membranes (the solid lines represent the pore transport model predictions with the optimized parameters); (b) Pore size distribution curve using PEGs as solute; (c) Cumulative pore size distribution for typical membranes

Table 3 Parameters for PSf-PEI/PDA and PSf-PEI/PDA/ECH membranes analyzed with VB_{12} and PEG rejections*

Membrane	d_p (nm)	$\Delta x/A_k$ (μm)	μ_p (nm)	σ_p	Pore size cutoff (nm)
PSf-PEI/PDA	2.53	5.9	1.5	1.65	2.94
PSf-PEI/PDA/ECH	1.68	9.1	1.1	1.60	1.87

* d_p and $\Delta x/A_k$ are determined from VB_{12} rejection and water permeance data; μ_p , σ_p , and pore size cut-off are calculated from PEG rejection data

was close to d_p , which indicates the reliability of using VB_{12} and PEGs for characterizing membrane pore size.

The influence of operating pressure on the flux and rejection of the DA/PEI/ECH-PSf membrane is shown in Fig. 9a. The permeation flux increased with increasing operating pressure as the pressure applied across the membrane increased. This can be explained by the Hagen-Poiseuille equation which shows that flux is proportional to the effective pressure driving force (Eq. (6)).

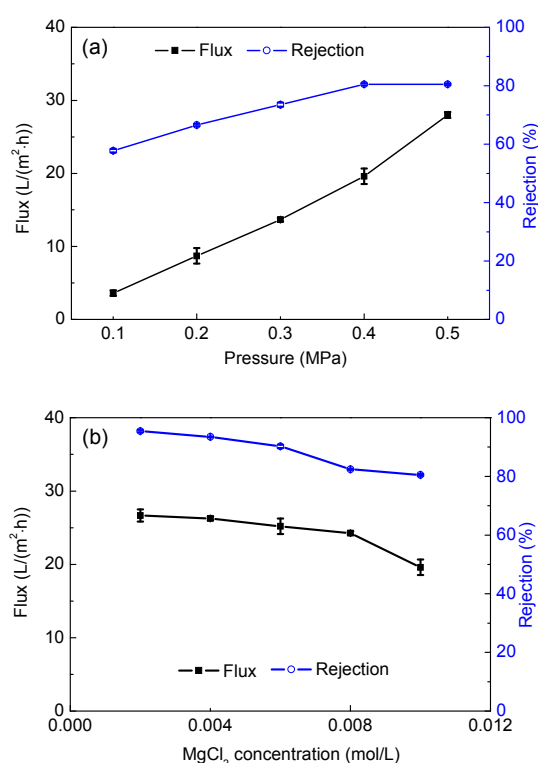


Fig. 9 Effects of operation pressure (a) and salt concentration (b) on the NF performance of the membranes

In addition, the rejection of salts reaches a plateau with increasing pressure. This can be explained by the Donnan-steric-pore-model (DSPM) and can be used to evaluate the contribution of each of transport mechanism. The solute flux includes contributions from diffusion (concentration gradient), electromigration (electrical potential gradient), and convection (pressure gradient) (Schaep *et al.*, 1999). When the pressure reaches a high level, diffusion contributes little as the permeate flux increases. Both convection

and electromigration are proportional to the pressure gradient. Therefore, the reduction in the diffusion effect may have contributed to the decrease in retention. The concentration of MgCl₂ had an obvious effect on both flux and rejection (Fig. 9b). The flux and rejection rate decreased with increasing concentrations of MgCl₂. This can be explained by the Donnan effect which states that the higher the concentration of salts, the weaker is the repulsion effect of the surface charged membrane. Osmotic pressure increases with increasing salt concentrations, resulting in a decrease in permeation flux.

3.4 Stability and durability of the membranes

The stability and durability of the composite membranes were examined by long-term filtration tests for 7 d. The results of permeation flux and rejection tests are shown in Fig. 10a. The flux and rejection showed little variation after long continuous tests. This stability may be due mainly to the interaction between the selective layer and the substrate strengthened by the co-deposition and cross-linking process. The composite membranes also showed good stability in acid and sodium hypochlorite solutions (Fig. 10b).

The stability of PDA particles in alkaline solution is usually considered to be poor at a pH of 11 (Dreyer *et al.*, 2012). More importantly, composite membranes modified by DA show poor tolerance to alkaline solutions over pH 11, which may be due to disassembly of PDA. However, washing and cleaning the membranes with alkaline solution is common practice in industry. The instability of the DA modified membrane is one of the reasons why this method cannot be developed for industrial applications. As the UV-vis spectra results shown in Fig. 10c, absorption at 280 nm is attributed to DA or a DA oligomer from the uncross-linked membrane surface after washing with an alkaline aqueous solution. This peak was not found in the cross-linked membranes, indicating that cross-linking had improved the stability of the membrane. The rejection rate of the composite membranes to MgCl₂ reduced little when they were immersed in alkaline solution (pH 12) after one day (Fig. 10d). After prolonging the washing time, the composite membranes showed little change in NF performance tests, indicating that the prepared

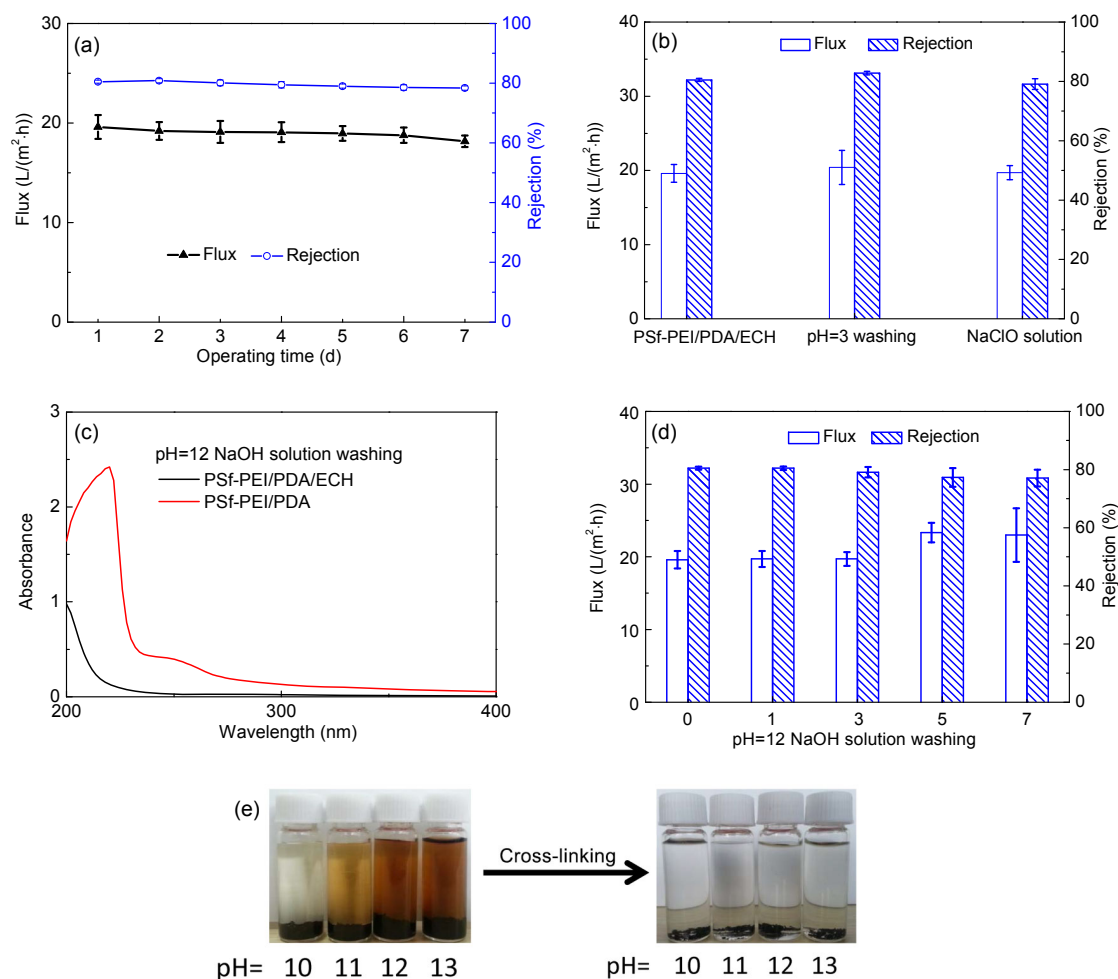


Fig. 10 (a) Effect of long NF tests on MgCl_2 rejection and water flux of PSf-PEI/PDA/ECH membranes; (b) NF tests after washing with pH=3 acid aqueous solutions and 500×10^{-6} NaClO solutions after 1 d; (c) UV-vis spectra of pH=12 NaOH solution after washing the cross-linked and uncross-linked membranes for 1 d; (d) NF tests after long washing with alkaline aqueous solution (pH=12); (e) Optical images of aggregates rinsed in alkaline solutions of different pH before and after cross-linking. MgCl_2 solution at a concentration of 0.01 mol/L under a test pressure of 0.4 MPa

membranes had good durability under such alkaline conditions. The PEI/PDA aggregates in solution were separated by centrifugation and then cross-linked by ECH. The stability of the uncross-linked and cross-linked aggregates was tested using alkaline solutions with various pH values (Fig 10e). The uncross-linked aggregates were partially dissociated at pH values over 11. However, not all the aggregates totally disappeared, indicating that the covalent bonding between PDA and PEI made it relatively stable. After a further covalent reactions caused by introducing ECH, the dissociation of aggregates was obviously inhibited, which is another indication of the good stability of the prepared composite membrane.

4 Conclusions

A composite NF membrane with a PDA-containing selective layer was successfully fabricated by DA-assisted PEI deposition on a PSf substrate followed by a cross-linking step. Self-polymerization and self-assembly of DA was strongly influenced by the introduction of PEI. Compared to the neat PDA-coated membranes, the composite NF membranes showed a higher rejection of divalent salts. The obtained membranes appeared to be positively charged, due to the introduction of PEI in the selective layer. The rejection of various salts followed the order $\text{MgCl}_2 \approx \text{CaCl}_2 > \text{MgSO}_4 > \text{NaCl} > \text{Na}_2\text{SO}_4$. Under

optimized preparation conditions, the salt rejection and permeation flux of the composite membranes reached up to 80.4% and 19.6 L/(m²·h), respectively (0.01 mol/L of MgCl₂ solution as the feed under a test pressure of 0.4 MPa). Significantly, the cross-linked PDA/PEI co-deposited selective layer showed improved durability in alkaline conditions compared to the uncross-linked system. The study revealed new opportunities for improving the tolerance of PDA-contained NF membranes to chemical cleaning.

References

- Akbari, A., Desclaux, S., Rouch, J.C., *et al.*, 2006. New UV-photografted nanofiltration membranes for the treatment of colored textile dye effluents. *Journal of Membrane Science*, **286**(1-2):342-350.
<http://dx.doi.org/10.1016/j.memsci.2006.10.024>
- Bouchoux, A., Roux-De Balman, H., Lutin, F., 2005. Nanofiltration of glucose and sodium lactate solutions. *Journal of Membrane Science*, **258**(1-2):123-132.
<http://dx.doi.org/10.1016/j.memsci.2005.03.002>
- Bowen, W.R., Mohammad, A.W., Hilal, N., 1997. Characterisation of nanofiltration membranes for predictive purposes—use of salts, uncharged solutes and atomic force microscopy. *Journal of Membrane Science*, **126**(1):91-105.
[http://dx.doi.org/10.1016/S0376-7388\(96\)00276-1](http://dx.doi.org/10.1016/S0376-7388(96)00276-1)
- Chan, E.P., Lee, J.H., Chung, J.Y., *et al.*, 2012. An automated spin-assisted approach for molecular layer-by-layer assembly of crosslinked polymer thin films. *Review of Scientific Instruments*, **83**(11):114102.
<http://dx.doi.org/10.1063/1.4767289>
- Chen, J., Chen, X., Yin, X., *et al.*, 2009. Bioinspired fabrication of composite pervaporation membranes with high permeation flux and structural stability. *Journal of Membrane Science*, **344**(1-2):136-143.
<http://dx.doi.org/10.1016/j.memsci.2009.07.044>
- Cheng, C., Nie, S., Li, S., *et al.*, 2013. Biopolymer functionalized reduced graphene oxide with enhanced biocompatibility via mussel inspired coatings/anchors. *Journal of Materials Chemistry B*, **1**(3):265-275.
<http://dx.doi.org/10.1039/C2TB00025C>
- Della Vecchia, N.F., Avolio, R., Alfè, M., *et al.*, 2013. Building-block diversity in polydopamine underpins a multifunctional eumelanin-type platform tunable through a quinone control point. *Advanced Functional Materials*, **23**(10):1331-1340.
<http://dx.doi.org/10.1002/adfm.201202127>
- Dreyer, D.R., Miller, D.J., Freeman, B.D., *et al.*, 2012. Elucidating the structure of poly(dopamine). *Langmuir*, **28**(15):6428-6435.
<http://dx.doi.org/10.1021/la204831b>
- Feng, C., Xu, J., Li, M., *et al.*, 2014. Studies on a novel nanofiltration membrane prepared by cross-linking of polyethyleneimine on polyacrylonitrile substrate. *Journal of Membrane Science*, **451**:103-110.
<http://dx.doi.org/10.1016/j.memsci.2013.10.003>
- Ji, Y.L., An, Q.F., Zhao, Q., *et al.*, 2012. Novel composite nanofiltration membranes containing zwitterions with high permeate flux and improved anti-fouling performance. *Journal of Membrane Science*, **390-391**:243-253.
<http://dx.doi.org/10.1016/j.memsci.2011.11.047>
- Jiang, J.H., Zhu, L.P., Li, X.L., *et al.*, 2010. Surface modification of PE porous membranes based on the strong adhesion of polydopamine and covalent immobilization of heparin. *Journal of Membrane Science*, **364**(1-2):194-202.
<http://dx.doi.org/10.1016/j.memsci.2010.08.017>
- Jiang, J.H., Zhu, L.P., Zhu, L.J., *et al.*, 2011. Surface characteristics of a self-polymerized dopamine coating deposited on hydrophobic polymer films. *Langmuir*, **27**(23):14180-14187.
<http://dx.doi.org/10.1021/la202877k>
- Kang, S.M., Hwang, N.S., Yeom, J., *et al.*, 2012. One-step multipurpose surface functionalization by adhesive catecholamine. *Advanced Functional Materials*, **22**(14):2949-2955.
<http://dx.doi.org/10.1002/adfm.201200177>
- Kasemset, S., Lee, A., Miller, D.J., *et al.*, 2013. Effect of polydopamine deposition conditions on fouling resistance, physical properties, and permeation properties of reverse osmosis membranes in oil/water separation. *Journal of Membrane Science*, **425-426**:208-216.
<http://dx.doi.org/10.1016/j.memsci.2012.08.049>
- Lee, H., Dellatore, S.M., Miller, W.M., *et al.*, 2007. Mussel-inspired surface chemistry for multifunctional coatings. *Science*, **318**(5849):426-430.
<http://dx.doi.org/10.1126/science.1147241>
- Li, M., Xu, J., Chang, C.Y., *et al.*, 2014. Bioinspired fabrication of composite nanofiltration membrane based on the formation of DA/PEI layer followed by cross-linking. *Journal of Membrane Science*, **459**:62-71.
<http://dx.doi.org/10.1016/j.memsci.2014.01.038>
- Li, X.L., Zhu, L.P., Jiang, J.H., *et al.*, 2011a. Hydrophilic nanofiltration membranes with self-polymerized and strongly-adhered polydopamine as separating layer. *Chinese Journal of Polymer Science*, **30**(2):152-163 (in Chinese).
<http://dx.doi.org/10.1007/s10118-012-1107-5>
- Li, X.L., Zhu, L.P., Xu, Y.Y., *et al.*, 2011b. A novel positively charged nanofiltration membrane prepared from *N,N*-dimethylaminoethyl methacrylate by quaternization cross-linking. *Journal of Membrane Science*, **374**(1-2):33-42.
<http://dx.doi.org/10.1016/j.memsci.2011.03.006>
- Miller, M.D., Bruening, M.L., 2004. Controlling the nanofiltration properties of multilayer polyelectrolyte membranes through variation of film composition. *Langmuir*, **20**(26):11545-11551.
<http://dx.doi.org/10.1021/la0479859>

- Nghiem, L.D., Schäfer, A.I., Elimelech, M., 2004. Removal of natural hormones by nanofiltration membranes: measurement, modeling, and mechanisms. *Environmental Science & Technology*, **38**(6):1888-1896.
<http://dx.doi.org/10.1021/es034952r>
- Ouyang, L., Malaisamy, R., Bruening, M.L., 2008. Multilayer polyelectrolyte films as nanofiltration membranes for separating monovalent and divalent cations. *Journal of Membrane Science*, **310**(1-2):76-84.
<http://dx.doi.org/10.1016/j.memsci.2007.10.031>
- Riera-Torres, M., Gutierrez-Bouzan, C., Crespi, M., 2010. Combination of coagulation-flocculation and nanofiltration techniques for dye removal and water reuse in textile effluents. *Desalination*, **252**(1-3):53-59.
<http://dx.doi.org/10.1016/j.desal.2009.11.002>
- Saeki, D., Imanishi, M., Ohmukai, Y., et al., 2013. Stabilization of layer-by-layer assembled nanofiltration membranes by crosslinking via amide bond formation and siloxane bond formation. *Journal of Membrane Science*, **447**:128-133.
<http://dx.doi.org/10.1016/j.memsci.2013.07.022>
- Schaep, J., Vandecasteele, C., 2001. Evaluating the charge of nanofiltration membranes. *Journal of Membrane Science*, **188**(1):129-136.
[http://dx.doi.org/10.1016/S0376-7388\(01\)00368-4](http://dx.doi.org/10.1016/S0376-7388(01)00368-4)
- Schaep, J., van der Bruggen, B., Vandecasteele, C., et al., 1998. Influence of ion size and charge in nanofiltration. *Separation and Purification Technology*, **14**(1-3):155-162.
[http://dx.doi.org/10.1016/S1383-5866\(98\)00070-7](http://dx.doi.org/10.1016/S1383-5866(98)00070-7)
- Schaep, J., Vandecasteele, C., Peeters, B., et al., 1999. Characteristics and retention properties of a mesoporous γ - Al_2O_3 membrane for nanofiltration. *Journal of Membrane Science*, **163**(2):229-237.
[http://dx.doi.org/10.1016/S0376-7388\(99\)00163-5](http://dx.doi.org/10.1016/S0376-7388(99)00163-5)
- Singh, S., Khulbe, K.C., Matsuura, T., et al., 1998. Membrane characterization by solute transport and atomic force microscopy. *Journal of Membrane Science*, **142**(1):111-127.
- Szymczyk, A., Fievet, P., 2005. Investigating transport properties of nanofiltration membranes by means of a steric, electric and dielectric exclusion model. *Journal of Membrane Science*, **252**(1-2):77-88.
<http://dx.doi.org/10.1016/j.memsci.2004.12.002>
- Tian, Y., Su, B., Jiang, L., 2014. Interfacial material system exhibiting superwettability. *Advanced Materials*, **26**(40):6872-6897.
<http://dx.doi.org/10.1002/adma.201400883>
- van der Bruggen, B., Schaep, J., Wilms, D., et al., 2000. A comparison of models to describe the maximal retention of organic molecules in nanofiltration. *Separation Science and Technology*, **35**(2):169-182.
<http://dx.doi.org/10.1081/SS-100100150>
- Vanherck, K., Vandezande, P., Aldea, S.O., et al., 2008. Cross-linked polyimide membranes for solvent resistant nanofiltration in aprotic solvents. *Journal of Membrane Science*, **320**(1-2):468-476.
<http://dx.doi.org/10.1016/j.memsci.2008.04.026>
- Xu, L.Q., Yang, W.J., Neoh, K.G., et al., 2010. Dopamine-induced reduction and functionalization of graphene oxide nanosheets. *Macromolecules*, **43**(20):8336-8339.
<http://dx.doi.org/10.1021/ma101526k>
- Yang, H.C., Liao, K.J., Huang, H., et al., 2014. Mussel-inspired modification of a polymer membrane for ultra-high water permeability and oil-in-water emulsion separation. *Journal of Materials Chemistry A*, **2**(26):10225-10230.
<http://dx.doi.org/10.1039/c4ta00143e>
- Zeman, L.J., Zydney, A.L., 1996. Microfiltration and Ultrafiltration: Principles and Applications. Marcel Dekker, New York, USA.
- Zhao, N., Wang, Z., Cai, C., et al., 2014. Bioinspired materials: from low to high dimensional structure. *Advanced Materials*, **26**(41):6994-7017.
<http://dx.doi.org/10.1002/adma.201401718>
- Zhou, M., Nemade, P.R., Lu, X., et al., 2007. New type of membrane material for water desalination based on a cross-linked bicontinuous cubic lyotropic liquid crystal assembly. *Journal of the American Chemical Society*, **129**(31):9574-9575.
<http://dx.doi.org/10.1021/ja073067w>

中文概要

题目：多巴胺辅助聚乙烯亚胺沉积交联的复合纳滤膜制备

目的：利用多巴胺改性构建一种简单制备荷正电复合纳滤膜，解决多巴胺类改性材料耐碱性差的问题。

创新点：1. 利用共沉积技术与交联反应成功制备了荷正电复合纳滤膜；相较于传统多巴胺改性膜，该复合膜的稳定性大大提高。2. 经过测试表征，制备得到的纳滤膜的分离尺寸属于疏松纳滤膜范围，可用于相应尺度的分离领域。

方法：1. 通过多巴胺与聚乙烯亚胺共沉积，首先实现二者的表面沉积，随后通过交联剂交联制备复合膜（图1）；2. 对改性膜前后表面理化性质进行相应表征（表2和图3~6）；3. 通过测试通量和截留等性能及分析相关纳滤模型，表征该复合膜分离性能（图7和8，公式（5）和（7））；4. 通过长期分离测试及碱性溶液清洗，测试复合膜的稳定性和耐碱性。

结论：1. 成功制备了具有荷正电性的复合纳滤膜；2. 通过通量和截留数据拟合分析得出该膜截留尺寸在1.5 nm和2 nm之间，属于疏松纳滤膜，可用于相应尺度分离；3. 该复合膜具有良好的稳定性及耐碱性，应用范围更广。

关键词：多巴胺；共沉积；纳滤膜；耐碱性